A combined neutron and x-ray diffraction study of short- and intermediate-range structural characteristics of Ge–As sulfide glasses

2008 J. Phys.: Condens. Matter 20 335105

(http://iopscience.iop.org/0953-8984/20/33/335105)

IOP PUBLISHING JOURNAL OF PHYSICS: CONDENSED MATTER

J. Phys.: Condens. Matter **20** (2008) 335105 (11pp) doi:10.1088/0953-8984/20/33/335105

A combined neutron and x-ray diffraction study of short- and intermediate-range structural characteristics of Ge–As sulfide glasses

S Soyer Uzun[1], S Sen[1,4], C J Benmore[2] and B G Aitken[3]

[1] Department of Chemical Engineering and Materials Science, University of California at Davis, Davis, CA 95616, USA
[2] Argonne National Laboratory, Argonne, IL 60439, USA
[3] Glass Research Division, Corning Incorporated, Corning, NY 14831, USA

E-mail: sbsen@ucdavis.edu

Received 2 March 2008, in final form 21 May 2008
Published 22 July 2008
Online at stacks.iop.org/JPhysCM/20/335105

Abstract

A combination of neutron and x-ray diffraction has been employed to study the compositional dependence of the atomic structures of $Ge_xAs_xS_{100-2x}$ glasses with S concentration varying between 33.3 and 70.0 at.%. The nearest-neighbor coordination numbers of Ge and As atoms are always found to be 4 and 3, respectively, irrespective of the glass composition. Ge and As atoms have primarily heteropolar bonding to S atoms in stoichiometric and S-excess glasses with $x \leqslant 18.2$. Low and intermediate levels of deficiency of S ($20 \leqslant x \leqslant 25$) are accommodated via the formation of homopolar As–As bonds while Ge atoms remain primarily bonded to four S atoms, resulting in As-rich regions in the glass structure. Ge starts to participate in metal–metal bonding only in the highly S-deficient glasses with $27.5 \leqslant x \leqslant 33.3$. The intermediate-range order and its topological influence on atomic packing in these three compositional regions, in the order of increasing deficiency in S, are controlled by (a) a mixed GeS_2 and As_2S_3 network, (b) the coexistence of a GeS_2 network and As clusters, and (c) large Ge–As metal-rich regions. This evolution of the intermediate-range structure with composition is consistent with the corresponding variation of the position, intensity and width of the first sharp diffraction peak in the structure factor.

1. Introduction

Chalcogenide glasses in binary and multicomponent systems are technologically important materials for applications in various active and passive photonic devices including optical fiber amplifiers, infrared lenses and windows and nonlinear optical components [1–3]. The short-and intermediate-range atomic structure of simple binary chalcogenide glasses in As–X, P–X and Ge–X (X = S, Se) systems have been studied in detail using various spectroscopic and diffraction techniques [3–14]. However, structural studies of complex glasses in the ternary and quaternary Ge–As–S/Se/Te glass-forming systems have focused primarily on short-range order [15–20]. Previous combined Ge and As K-edge EXAFS spectroscopy results indicated that the covalent network structure of complex ternary and quaternary Ge–As–S, Se glasses with stoichiometric and S(Se)-excess compositions consist of corner-sharing $GeS(Se)_4$ tetrahedra and $AsS(Se)_3$ trigonal pyramids [15–17]. On the other hand, as S(Se)-deficiency increases the formation of metal–metal bonds take place between Ge and As atoms in the structure while the nearest-neighbor coordination numbers of Ge and As atoms remain 4 and 3, respectively, independent of chemical composition. Although such detailed information on short-range order is available for these glasses, direct experimental studies of structural characteristics beyond the nearest-neighbor length scale remain lacking. Such studies

[4] Author to whom any correspondence should be addressed.

Table 1. Compositions and glass transition temperatures of $Ge_xAs_xS_{100-2x}$ glasses used in this study.

Chemical composition (±0.1 at.%)	%S in excess of stoichiometry	T_g (°C)
$Ge_{15}As_{15}S_{70}$	33.3	178
$Ge_{18.2}As_{18.2}S_{63.6}$	0.0	297
$Ge_{20}As_{20}S_{60}$	−14.3	312
$Ge_{22.5}As_{22.5}S_{55}$	−30.2	337
$Ge_{25}As_{25}S_{50}$	−42.9	363
$Ge_{27.5}As_{27.5}S_{45}$	−53.3	390
$Ge_{30}As_{30}S_{40}$	−61.9	434
$Ge_{32.5}As_{32.5}S_{35}$	−69.2	443
$Ge_{33.3}As_{33.3}S_{33.3}$	−71.4	435

are particularly difficult as structural interpretation of the diffraction data for multicomponent glasses becomes strongly model-dependent and non-unique due to the convolution of a large number of pair-correlation functions in the radial distribution function (RDF). This difficulty can be partially overcome by following the evolution of the RDF as a function of systematic variation in glass composition within a glass-forming system. Furthermore, combined neutron and x-ray diffraction can be used to decipher the contributions from various pair-correlation functions in the RDF since neutrons and x-rays often weigh pair-correlations differently. In this study, a combination of neutron and high-energy x-ray diffraction has been employed to obtain a detailed picture of compositional evolution of the short- and intermediate-range structural characteristics of $Ge_xAs_xS_{100-2x}$ chalcogenide glasses with $15 \leqslant x \leqslant 33.3$. The interrelationships between the nature and characteristic length scales of these structural characteristics are also addressed.

2. Experimental details

2.1. Sample synthesis

Ge–As sulfide glasses reported in this study were synthesized by melting mixtures of the constituent elements Ge, As and S with ⩾99.995% purity (metals basis) in evacuated (10^{-6} Torr) and flame sealed fused silica ampoules at ∼1200 K for at least 24 h in a rocking furnace. The ampoules were quenched in water and subsequently annealed for 1 h at the respective glass transition temperatures. A more detailed description of the preparation method can be found elsewhere [19]. The chemical compositions and calorimetric glass transition temperatures of the $Ge_xAs_xS_{100-2x}$ glasses are listed in table 1.

2.2. Data collection

Neutron diffraction experiments were carried out using the glass, liquid, and amorphous materials diffractometer (GLAD) at the intense pulsed neutron source (IPNS) at Argonne National Laboratory [21]. Crushed glass samples were taken in 9.5 mm diameter cylindrical vanadium cans and data were collected over a Q range of 0.2–40.0 Å^{-1}. The beam size was 4 × 4 cm^2 and the duration of the data collection for each sample was ∼18 h. High-energy x-ray diffraction experiments were performed on the 11-IDC beamline at the Advanced Photon Source (APS) at Argonne National Laboratory. Crushed samples were taken in 2.5 mm diameter cylindrical SiO_2 capillaries with wall thickness of 100 μm. Data were collected over a Q range of 0.3–25.0 Å^{-1} using a solid-state Ge detector. An incident photon energy of 115.47 keV ($\lambda = 0.107\,375$ Å) was used. The beam size was 1 × 3 mm^2 and the duration of the data collection for each sample was ∼14 h.

2.3. Data processing

Neutron diffraction data were corrected using standard procedures for container and background scattering, absorption, multiple scattering and inelasticity effects, and were normalized to an absolute scale with the isotropic incoherent scattering from vanadium. The resulting total scattering structure factor $F_N(Q)$ is related to the total neutron static structure factor $S_N(Q)$ via the following expression:

$$S_N(Q) = \frac{F_N(Q)}{(\sum_i c_i b_i)^2} = \frac{1}{(\sum_i c_i b_i)^2} \sum_{i,j} c_i b_i c_j b_j (S_{ij}(Q) - 1) \quad (1)$$

where c_i is the atomic concentration and b_i is the neutron scattering length of species i = As, Ge, S (6.58, 8.18 and 2.85 fm, respectively) and $S_{ij}(Q)$ are the Faber–Ziman partial structure factors [22, 23]. A Q-range of 0.3–25 Å^{-1} was used along with the Lorch modification function [24] for the Fourier transformation of the $S_N(Q)$ data.

The high-energy x-ray data were reduced using standard procedures and the software analysis package *ISOMER-X* [22]. Corrections were made for background, sample-holder scattering and absorption and the scattering intensities were normalized to the sum of elastic plus Compton scattering. Finally the Compton scattering function was subtracted to obtain the total x-ray static structure factors $S_X(Q)$. In x-ray diffraction, within independent atom approximation, $S_X(Q)$ can be expressed as:

$$S_X(Q) = \frac{I_X(Q)}{(\sum_i c_i f_i(Q))^2} = \frac{1}{(\sum_i c_i f_i(Q))^2} \times \sum_{i,j} c_i f_i(Q) c_j f_j(Q) (S_{ij}(Q) - 1) \quad (2)$$

where $I_X(Q)$ is the distinct scattering, $f_i(Q)$ are the Q-dependent neutral atom form factors [25].

The total structure factor $S_{N(X)}(Q)$ is related to the neutron (x-ray) total radial distribution function, $N(r)$, via Fourier transformation. The Fourier transformation of the $S_X(Q)$ data was carried out using the same Lorch modification function and Q-range (0.3–25 Å^{-1}) as those used for the Fourier transformation of the $S_N(Q)$ data (see above).

The total neutron (x-ray) radial distribution function $N(r)$ is given by:

$$N(r) = 4\pi r^2 \rho_0 g(r) \quad (3)$$

where ρ_0 is the total number density and $g(r)$ is a weighted average of the partial pair distribution functions $g_{ij}(r)$ for the

atom pair i and j and is given by:

$$g(r) = \frac{1}{\langle b\rangle^2}\sum_{ij} c_i c_j b_i b_j g_{ij}(r)$$

for neutron diffraction and

$$g(r) = \sum_{ij}\frac{c_i c_j f_i(Q) f_j(Q) g_{ij}(r)}{\langle f(Q)\rangle^2}$$

for x-ray diffraction where $\langle b\rangle^2$ is $(\sum_i c_i b_i)^2$ and $\langle f(Q)\rangle^2$ is $[\sum_i c_i f_i(Q)]^2$. The quantities

$$\frac{(2-\partial)\, c_i c_j b_i b_j}{\langle b\rangle^2}$$

and

$$\frac{(2-\partial)\, c_i c_j f_i(Q) f_j(Q)}{\langle f(Q)\rangle^2}$$

(where $\partial = 1$ for $i = j$ and $\partial = 0$ for $i \neq j$) are the Faber–Ziman weighting factors w_{ij}^{N} and w_{ij}^{X} for neutron and x-ray, respectively, and are tabulated in table 2a for all glass compositions studied here. The double counting of the weighting factors for $i \neq j$ takes into account of the fact that contributions from partial pair distribution functions $g_{ij}(r)$ and $g_{ji}(r)$ are identical. The quantity w_{ij}^{X} has been approximated to be independent of Q in the subsequent discussion.

$N(r)\,\mathrm{d}r$ has a direct physical interpretation as the number of atoms that are present within a range $(r, r+\mathrm{d}r)$ from any given atom [26, 27]. A weighted average coordination number for a peak in neutron (x-ray) $N(r)$ extending from r_1 to r_2 can be described as:

$$C^{\mathrm{N(X)}} = \int_{r_1}^{r_2} N_{\mathrm{N(X)}}(r)\,\mathrm{d}r. \tag{4}$$

In a neutron diffraction experiment C^{N} can be related to the partial coordination numbers $C_i(j)$ expressing the average number of j atoms within this r range from an i atom at the center:

$$C^{\mathrm{N}} = \frac{1}{\langle b\rangle^2}\sum_{ij} c_i b_i b_j C_i(j). \tag{5}$$

For the Ge–As–S ternary system equation (5) becomes:

$$\begin{aligned} C^{\mathrm{N}} = {} & c_{\mathrm{Ge}}\frac{b_{\mathrm{Ge}}^2}{\langle b\rangle^2}C_{\mathrm{Ge}}(\mathrm{Ge}) + 2c_{\mathrm{Ge}}\frac{b_{\mathrm{Ge}}b_{\mathrm{As}}}{\langle b\rangle^2}C_{\mathrm{Ge}}(\mathrm{As}) \\ & + 2c_{\mathrm{Ge}}\frac{b_{\mathrm{Ge}}b_{\mathrm{S}}}{\langle b\rangle^2}C_{\mathrm{Ge}}(\mathrm{S}) + c_{\mathrm{As}}\frac{b_{\mathrm{As}}^2}{\langle b\rangle^2}C_{\mathrm{As}}(\mathrm{As}) \\ & + 2c_{\mathrm{As}}\frac{b_{\mathrm{As}}b_{\mathrm{S}}}{\langle b\rangle^2}C_{\mathrm{As}}(\mathrm{S}) + c_{\mathrm{S}}\frac{b_{\mathrm{S}}^2}{\langle b\rangle^2}C_{\mathrm{S}}(\mathrm{S}). \end{aligned} \tag{6}$$

Equation (6) can be written as:

$$\begin{aligned} C^{\mathrm{N}} = {} & W_{\mathrm{GeGe}}^{\mathrm{N}}C_{\mathrm{Ge}}(\mathrm{Ge}) + W_{\mathrm{GeAs}}^{\mathrm{N}}C_{\mathrm{Ge}}(\mathrm{As}) + W_{\mathrm{GeS}}^{\mathrm{N}}C_{\mathrm{Ge}}(\mathrm{S}) \\ & + W_{\mathrm{AsAs}}^{\mathrm{N}}C_{\mathrm{As}}(\mathrm{As}) + W_{\mathrm{AsS}}^{\mathrm{N}}C_{\mathrm{As}}(\mathrm{S}) + W_{\mathrm{SS}}^{\mathrm{N}}C_{\mathrm{S}}(\mathrm{S}) \end{aligned} \tag{7}$$

where W_{ij}^{N} are the neutron weighting factors representing the contribution of each of the partial $C_i(j)$ to C^{N} [26].

In an x-ray diffraction experiment, the relation between C^{X} and the partial coordination numbers $C_i(j)$ can be given as:

$$C^{\mathrm{X}} = \frac{1}{\langle f(0)\rangle^2}\sum_{ij} c_i Z_i Z_j C_i(j) \tag{8}$$

where $\langle f(0)\rangle^2$ is the average neutral atom x-ray form factor at $Q = 0$ Å^{-1} and is given by $(\sum_i c_i Z_i)^2$ where Z_i is the number of electrons of species i = As, Ge, S (33, 32 and 16, respectively).

For the Ge–As–S system, equation (8) becomes:

$$\begin{aligned} C^{\mathrm{X}} = {} & c_{\mathrm{Ge}}\frac{Z_{\mathrm{Ge}}^2}{\langle f(0)\rangle^2}C_{\mathrm{Ge}}(\mathrm{Ge}) + 2c_{\mathrm{Ge}}\frac{Z_{\mathrm{Ge}}Z_{\mathrm{As}}}{\langle f(0)\rangle^2}C_{\mathrm{Ge}}(\mathrm{As}) \\ & + 2c_{\mathrm{Ge}}\frac{Z_{\mathrm{Ge}}Z_{\mathrm{S}}}{\langle f(0)\rangle^2}C_{\mathrm{Ge}}(\mathrm{S}) + c_{\mathrm{As}}\frac{Z_{\mathrm{As}}^2}{\langle f(0)\rangle^2}C_{\mathrm{As}}(\mathrm{As}) \\ & + 2c_{\mathrm{As}}\frac{Z_{\mathrm{As}}Z_{\mathrm{S}}}{\langle f(0)\rangle^2}C_{\mathrm{As}}(\mathrm{S}) + c_{\mathrm{S}}\frac{Z_{\mathrm{S}}^2}{\langle f(0)\rangle^2}C_{\mathrm{S}}(\mathrm{S}). \end{aligned} \tag{9}$$

In equations (6) and (9) contributions from $C_i(j)$ terms for hetero-atom pairs where $i \neq j$ have been counted twice to take into account the contributions from both the terms $C_i(j)$ and $C_j(i)$. Equation (9) can be written in terms of x-ray weighting factors as:

$$\begin{aligned} C^{\mathrm{X}} = {} & W_{\mathrm{GeGe}}^{\mathrm{X}}C_{\mathrm{Ge}}(\mathrm{Ge}) + W_{\mathrm{GeAs}}^{\mathrm{X}}C_{\mathrm{Ge}}(\mathrm{As}) + W_{\mathrm{GeS}}^{\mathrm{X}}C_{\mathrm{Ge}}(\mathrm{S}) \\ & + W_{\mathrm{AsAs}}^{\mathrm{X}}C_{\mathrm{As}}(\mathrm{As}) + W_{\mathrm{AsS}}^{\mathrm{X}}C_{\mathrm{As}}(\mathrm{S}) + W_{\mathrm{SS}}^{\mathrm{X}}C_{\mathrm{S}}(\mathrm{S}) \end{aligned} \tag{10}$$

where W_{ij}^{X} are the x-ray weighting factors representing the contribution of each of the partial $C_i(j)$ to C^{X} [26].

Neutron and x-ray diffraction can be used as complementary techniques due to the contrast resulting from the differences in the neutron and x-ray weighting factors of various partials $C_i(j)$. These weighting factors for all glass compositions are listed in table 2b. Thus, a combination of equations (7) and (10) is used to solve for the nearest-neighbor coordination environments in the $\mathrm{Ge}_x\mathrm{As}_x\mathrm{S}_{100-2x}$ glasses.

3. Results

The experimental neutron and x-ray structure factors $S_{\mathrm{N}}(Q)$ and $S_{\mathrm{X}}(Q)$ are shown in figures 1 and 2. The corresponding neutron and x-ray radial distribution functions $N(r)$ for all $\mathrm{Ge}_x\mathrm{As}_x\mathrm{S}_{100-2x}$ glasses are shown in figures 3 and 4, respectively.

3.1. First sharp diffraction peak

A linear function is used to approximate the local background underneath the first sharp diffraction peaks (FSDP) in $S_{\mathrm{N}}(Q)$ and $S_{\mathrm{X}}(Q)$, thus allowing the FSDP to be isolated and fitted with a Gaussian or Lorentzian function. Although the peak shape could not be exactly reproduced with either function, somewhat better fits were obtained with Gaussian functions for most cases. Therefore, Gaussian fits were used to extract the position, width and intensity parameters for the FSDP in all cases (table 3). The position, width and intensity of the x-ray and neutron FSDP exhibit systematic changes with glass composition (figures 5, 6, table 3). These parameters exhibit similar trends for both x-ray and neutron. The position of the neutron FSDP is located at 1.15 Å^{-1} for the S-excess $\mathrm{Ge}_{15}\mathrm{As}_{15}\mathrm{S}_{70}$ glass and it monotonically shifts to lower Q values with decreasing S content until it is located at 0.97 Å^{-1} for the most S-deficient $\mathrm{Ge}_{33.3}\mathrm{As}_{33.3}\mathrm{S}_{33.3}$ glass (figure 5). The positions of the x-ray FSDPs exhibits a similar trend, however,

Table 2a. Normalized Faber–Ziman neutron (N) and x-ray (X) weighting factors for $Ge_xAs_xS_{100-2x}$ glasses. X-ray values have been calculated at $Q = 0$ Å^{-1}.

Chemical composition	Ge–Ge	Ge–As	Ge–S	As–As	As–S	S–S	
$Ge_{15}As_{15}S_{70}$	0.085	0.137	0.276	0.055	0.222	0.224	N
	0.053	0.108	0.245	0.056	0.253	0.286	X
$Ge_{18.2}As_{18.2}S_{63.6}$	0.110	0.176	0.267	0.071	0.214	0.162	N
	0.070	0.144	0.245	0.074	0.252	0.213	X
$Ge_{20}As_{20}S_{60}$	0.123	0.198	0.257	0.080	0.207	0.134	N
	0.080	0.165	0.241	0.085	0.248	0.180	X
$Ge_{22.5}As_{22.5}S_{55}$	0.142	0.228	0.241	0.092	0.194	0.103	N
	0.094	0.195	0.231	0.100	0.238	0.141	X
$Ge_{25}As_{25}S_{50}$	0.160	0.257	0.222	0.103	0.179	0.077	N
	0.109	0.224	0.218	0.116	0.224	0.109	X
$Ge_{27.5}As_{27.5}S_{45}$	0.178	0.286	0.202	0.115	0.163	0.058	N
	0.123	0.254	0.202	0.131	0.208	0.082	X
$Ge_{30}As_{30}S_{40}$	0.194	0.313	0.180	0.126	0.145	0.042	N
	0.137	0.283	0.183	0.146	0.189	0.061	X
$Ge_{32.5}As_{32.5}S_{35}$	0.211	0.339	0.158	0.136	0.127	0.030	N
	0.151	0.312	0.163	0.161	0.168	0.044	X
$Ge_{33.3}As_{33.3}S_{33.3}$	0.216	0.347	0.150	0.140	0.121	0.026	N
	0.156	0.322	0.156	0.166	0.161	0.039	X

Table 2b. Neutron (N) and x-ray (X) weighting factors (W_{ij}) for $Ge_xAs_xS_{100-2x}$ glasses defining the contribution of each of partial $C_i(j)$ to C^N and C^X (see text for details).

Chemical composition	Ge–Ge	Ge–As	Ge–S	As–As	As–S	S–S	
$Ge_{15}As_{15}S_{70}$	0.568	0.913	0.395	0.367	0.317	0.320	N
	0.350	0.722	0.350	0.372	0.361	0.408	X
$Ge_{18.2}As_{18.2}S_{63.6}$	0.603	0.969	0.419	0.389	0.337	0.255	N
	0.385	0.794	0.385	0.409	0.397	0.336	X
$Ge_{20}As_{20}S_{60}$	0.617	0.992	0.429	0.399	0.345	0.224	N
	0.401	0.827	0.401	0.426	0.414	0.301	X
$Ge_{22.5}As_{22.5}S_{55}$	0.631	1.014	0.439	0.408	0.353	0.187	N
	0.420	0.866	0.420	0.447	0.433	0.257	X
$Ge_{25}As_{25}S_{50}$	0.640	1.029	0.445	0.414	0.358	0.155	N
	0.435	0.898	0.435	0.463	0.449	0.218	X
$Ge_{27.5}As_{27.5}S_{45}$	0.646	1.038	0.449	0.417	0.361	0.128	N
	0.448	0.924	0.448	0.476	0.462	0.183	X
$Ge_{30}As_{30}S_{40}$	0.648	1.042	0.451	0.419	0.363	0.105	N
	0.458	0.944	0.458	0.487	0.472	0.153	X
$Ge_{32.5}As_{32.5}S_{35}$	0.648	1.042	0.451	0.419	0.363	0.084	N
	0.466	0.961	0.466	0.496	0.481	0.125	X
$Ge_{33.3}As_{33.3}S_{33.3}$	0.649	1.043	0.451	0.419	0.363	0.078	N
	0.469	0.967	0.469	0.498	0.483	0.117	X

these positions are located at slightly lower Q values compared to those of the neutron FSDPs (figure 5, table 3). On the other hand, the intensities of the neutron and x-ray FSDPs rise sharply with increasing S-deficiency, both reaching a maximum at $x = 20$. The intensity of the neutron FSDP stays somewhat constant in the compositional region of $20 \leqslant x \leqslant 25$ while the x-ray FSDP intensity values decrease in this region. Both x-ray and neutron FSDP intensities rapidly decreases with further increase in S-deficiency in the compositional region of $25 \leqslant x \leqslant 33.3$ (figure 5). The widths of the neutron and x-ray FSDPs decrease monotonically with increasing S-deficiency in the composition range $15 \leqslant x \leqslant 25$ beyond which it increases somewhat with further decrease in the S content down to $x = 33.3$ (figure 6). The minor but systematic differences between the x-ray and neutron FSDP parameters, as evident in figures 5 and 6, possibly arise from the differences in the neutron and x-ray scattering cross-sections of the constituent elements. It is also interesting to note that the lowest-Q ($Q \leqslant 0.30$ Å^{-1}) part of the $S_N(Q)$ for S-deficient glasses ($x > 0.182$) display significant small-angle scattering (figure 1(b)). The intensity of small-angle scattering increases with decreasing S content up to $x = 30$ and then decreases with further increase in x. Such small-angle scattering was not observed in the $S_X(Q)$ as the $S_X(Q)$ data do not extend below $Q = 0.30$ Å^{-1} due to the cutoff from a low-Q beam stop.

Table 3. FSDP parameters of $Ge_xAs_xS_{100-2x}$ glasses used in this study.

	FSDP parameters					
	Neutron			X-ray		
Chemical composition	Position ($Å^{-1}$)	Intensity	Width ($Å^{-1}$)	Position ($Å^{-1}$)	Intensity	Width ($Å^{-1}$)
$Ge_{15}As_{15}S_{70}$	1.153 ± 0.001	0.819 ± 0.007	0.334 ± 0.004	1.144 ± 0.001	0.922 ± 0.005	0.340 ± 0.003
$Ge_{18.2}As_{18.2}S_{63.6}$	1.127 ± 0.001	0.975 ± 0.009	0.326 ± 0.004	1.129 ± 0.001	1.072 ± 0.009	0.336 ± 0.004
$Ge_{20}As_{20}S_{60}$	1.093 ± 0.002	1.174 ± 0.014	0.277 ± 0.004	1.065 ± 0.001	1.382 ± 0.012	0.288 ± 0.003
$Ge_{22.5}As_{22.5}S_{55}$	1.068 ± 0.001	1.160 ± 0.012	0.272 ± 0.004	1.043 ± 0.001	1.249 ± 0.011	0.270 ± 0.003
$Ge_{25}As_{25}S_{50}$	1.041 ± 0.001	1.157 ± 0.014	0.261 ± 0.004	1.032 ± 0.001	1.205 ± 0.010	0.270 ± 0.003
$Ge_{27.5}As_{27.5}S_{45}$	1.018 ± 0.002	1.060 ± 0.014	0.259 ± 0.004	1.003 ± 0.001	1.116 ± 0.011	0.276 ± 0.004
$Ge_{30}As_{30}S_{40}$	0.995 ± 0.002	0.917 ± 0.013	0.263 ± 0.005	0.978 ± 0.001	0.959 ± 0.011	0.284 ± 0.004
$Ge_{32.5}As_{32.5}S_{35}$	0.978 ± 0.003	0.770 ± 0.017	0.260 ± 0.007	0.960 ± 0.002	0.807 ± 0.010	0.288 ± 0.005
$Ge_{33.3}As_{33.3}S_{33.3}$	0.973 ± 0.001	0.739 ± 0.008	0.267 ± 0.004	0.957 ± 0.002	0.736 ± 0.010	0.290 ± 0.005

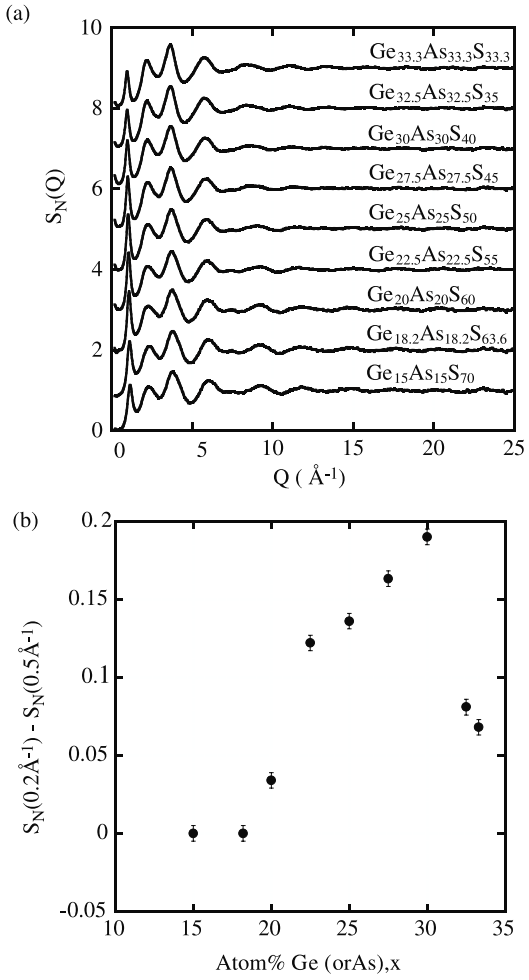

Figure 1. (a) Neutron total structure factors $S_N(Q)$ for $Ge_xAs_xS_{100-2x}$ glasses. The curves are vertically displaced for clarity. Corresponding glass compositions are shown alongside each curve. (b) Compositional dependence of the difference in intensity of $S_N(Q)$ at $Q = 0.2$ and 0.3 $Å^{-1}$ used as a measure of small-angle neutron scattering.

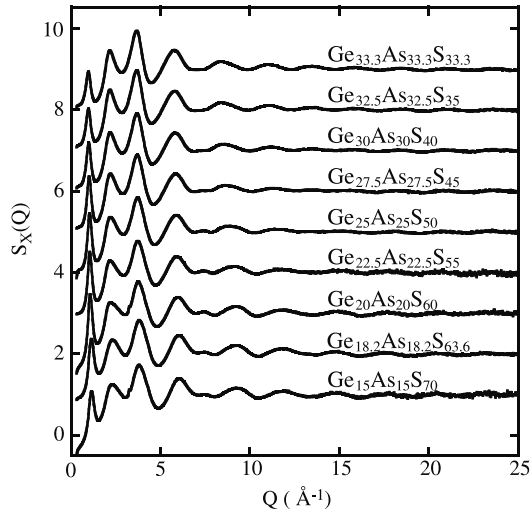

Figure 2. X-ray total structure factors $S_X(Q)$ for $Ge_xAs_xS_{100-2x}$ glasses. The curves are vertically displaced for clarity. Corresponding glass compositions are shown alongside each curve.

3.2. Radial distribution function

3.2.1. First shell and the nearest-neighbor coordination environments. The nearest-neighbor coordination environments of the Ge and As atoms in the structures of these glasses are represented by the peak(s) that are located between 2 and 3 Å in neutron and x-ray $N(r)$ (figures 3, 4). For the S-excess and stoichiometric glasses the peak located at ∼2.2 corresponds to both As–S and Ge–S nearest-neighbor distances [7–12, 15, 16]. It may be noted that this distance is in good agreement with the sum of the covalent radii of Ge–S (2.24 Å) and As–S (2.21 Å) atom pairs. A second peak at ∼2.5 Å appears in the $N(r)$ and grows progressively in intensity with increasing S-deficiencies (figures 3, 4). This peak can be readily assigned on the basis of its position to metal–metal nearest neighbors in S-deficient glasses [7–12, 15, 16]. The position of this peak agrees well with the sum of the covalent radii of Ge–Ge (2.45 Å), Ge–As (2.41 Å) and As–As (2.38 Å) atom pairs.

In the case of S-excess and stoichiometric glasses ($x \leqslant 18.2$) the total area C^N of the peak centered at 2.24 Å in neutron $N(r)$ (figure 3) corresponding to As–S and Ge–S correlations, can be expressed by reducing equation (7):

$$C^N = W^N_{AsS} C_{As}(S) + W^N_{GeS} C_{Ge}(S). \quad (11)$$

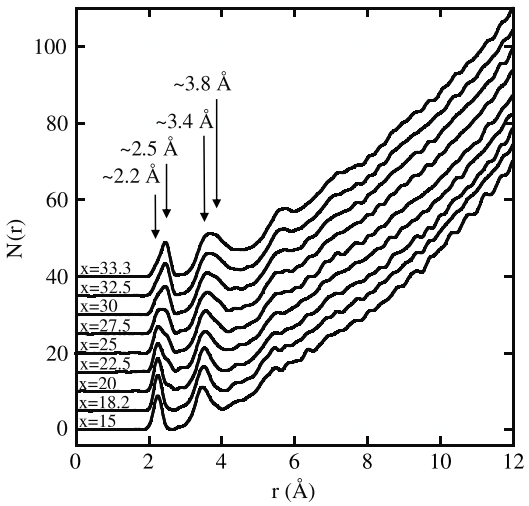

Figure 3. Neutron radial distribution functions $N(r)$ for $Ge_xAs_xS_{100-2x}$ glasses. These functions are obtained by the Fourier transformation of the $S_N(Q)$ data shown in figure 1(a). The curves are vertically displaced for clarity. Corresponding glass compositions are shown alongside each curve.

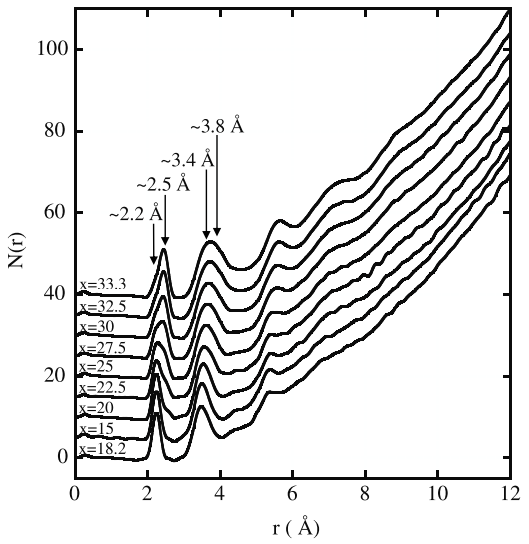

Figure 4. X-ray radial distribution functions $N(r)$ for $Ge_xAs_xS_{100-2x}$ glasses. These functions are obtained by the Fourier transformation of the $S_X(Q)$ data shown in figure 2. The curves are vertically displaced for clarity. Corresponding glass compositions are shown alongside each curve.

A similar equation can be written for x-ray by reducing equation (10) such that:

$$C^X = W^X_{AsS} C_{As}(S) + W^X_{GeS} C_{Ge}(S) \qquad (12)$$

where C^X is the total area of the peak located at 2.24 in x-ray $N(r)$.

For S-excess and stoichiometric glasses equations (11), and (12) were solved together. Thus, $C_{As}(S)$ and $C_{Ge}(S)$ were readily calculated to be ∼3 and 4, respectively without needing any additional constraints (table 4). These coordination numbers are consistent with the results of previous Ge and As K-edge EXAFS spectroscopic studies of these glasses [15, 16].

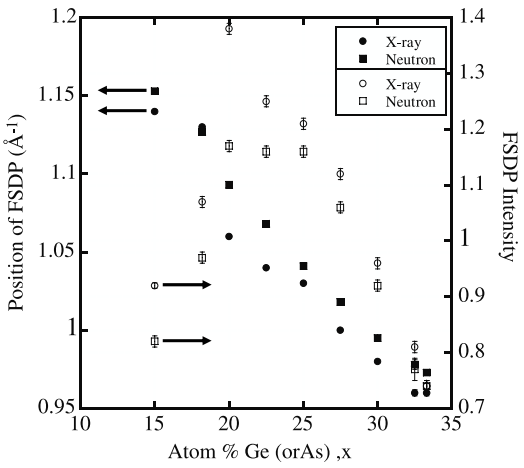

Figure 5. Variation in the position and intensity of the neutron and x-ray FSDP in $Ge_xAs_xS_{100-2x}$ glasses as a function of Ge (or As) content. Neutron (x-ray) FSDP position and intensity data are represented by filled and open squares (circles), respectively. Error bars for the FSDP position data are within the size of the symbols.

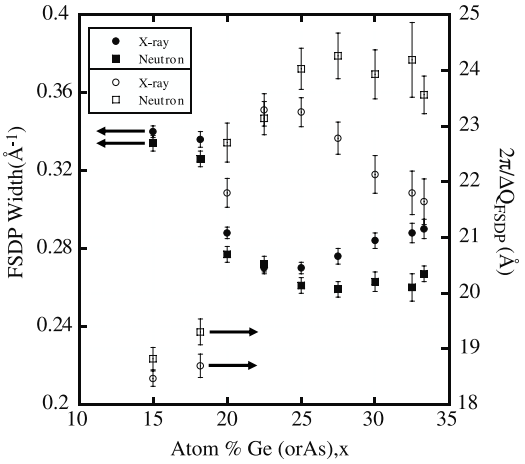

Figure 6. Variation in the width of the FSDP and the coherence length of intermediate-range order ($2\pi/\Delta Q_{FSDP}$) in $Ge_xAs_xS_{100-2x}$ glasses as a function of Ge (or As) content. Widths and coherence lengths related to neutron (x-ray) FSDP are represented by closed and open squares (circles), respectively.

A previous study of the Raman spectra of S-excess glasses in the Ge–As–S system exhibited a band near 490 cm^{-1} corresponding to the stretching vibration of S–S bonds [18]. The corresponding S–S bond length is expected to be ∼2.0 Å. However, this S–S correlation is not observed in the corresponding neutron and x-ray $N(r)$ of the S-excess glass which is consistent with the chemical composition of the S-excess glass that implies a rather weak weighting of this correlation in the total $g(r)$ resulting from a small average $C_S(S)$ of ∼0.5, provided $C_{Ge}(S) = 4.0$ and $C_{As}(S) = 3.0$.

Previous EXAFS studies of $Ge_xAs_xS_{100-2x}$ glasses with low and intermediate levels of S-deficiencies ($20 \leqslant x \leqslant 25$) have shown that that in this composition range only As atoms participate in metal–metal bonding while Ge atoms are primarily coordinated to 4 S atoms [15–17]. Therefore, for

Table 4. Inter-atomic distances and coordination numbers for Ge and As atoms in $Ge_xAs_xS_{100-2x}$ glasses.

	First coordination shell									
			Average Ge/As–S distance (Å)				Average As–As distance (Å)			
Composition	$C_{Ge}(S)$	$C_{As}(S)$	Neutron	X-ray	$C_{As}(As)$	$C_{As}(As)$[a]	Neutron	X-ray		
$Ge_{15}As_{15}S_{70}$	4.0 ± 0.2[b]	3.0 ± 0.2[b]	2.24 ± 0.01	2.24 ± 0.01	—	—	—	—		
$Ge_{18.2}As_{18.2}S_{63.6}$	4.0 ± 0.2[b]	3.0 ± 0.2[b]	2.24 ± 0.01	2.25 ± 0.01	—	—	—	—		
$Ge_{20}As_{20}S_{60}$	4.0	1.6 ± 0.4[c]	2.24 ± 0.01	2.24 ± 0.01	1.4 ± 0.3[c]	1.0	2.53 ± 0.01	2.46 ± 0.01		
$Ge_{22.5}As_{22.5}S_{55}$	4.0	1.3 ± 0.4[c]	2.23 ± 0.01	2.23 ± 0.01	1.7 ± 0.3[c]	2.1	2.49 ± 0.01	2.47 ± 0.01		
$Ge_{25}As_{25}S_{50}$	4.0	0.0 ± 0.3[c]	2.24 ± 0.01	2.23 ± 0.01	2.8 ± 0.2[c]	3.0	2.49 ± 0.01	2.46 ± 0.01		
					Case 1[e]		Case 2[f]		Average Ge/As–Ge/As distance (Å)	
			Neutron	X-ray	$C_{As}(As)$	$C_{Ge}(Ge)$	$C_{As}(As + Ge)$	$C_{Ge}(As)$	Neutron	X-ray
$Ge_{27.5}As_{27.5}S_{45}$	3.6 ± 0.1[d]	—	2.24 ± 0.1	2.24 ± 0.1	2.9 ± 0.1	0.5 ± 0.1	2.9 ± 0.1	0.7 ± 0.1	2.48 ± 0.1	2.46 ± 0.1
$Ge_{30}As_{30}S_{40}$	2.9 ± 0.1[d]	—	2.24 ± 0.1	2.25 ± 0.1	2.7 ± 0.1	1.1 ± 0.1	2.7 ± 0.1	1.3 ± 0.1	2.47 ± 0.1	2.47 ± 0.1
$Ge_{32.5}As_{32.5}S_{35}$	2.4 ± 0.1[d]	—	2.25 ± 0.1	2.27 ± 0.1	2.9 ± 0.1	1.3 ± 0.1	2.8 ± 0.1	1.4 ± 0.1	2.47 ± 0.1	2.47 ± 0.1
$Ge_{33.3}As_{33.3}S_{33.3}$	2.1 ± 0.1[d]	—	2.25 ± 0.1	2.29 ± 0.1	3.0 ± 0.1	1.9 ± 0.1	2.9 ± 0.1	1.6 ± 0.1	2.46 ± 0.1	2.47 ± 0.1

[a] As–As nearest-neighbor coordination numbers expected from stoichiometry for complete exclusion of Ge from metal–metal bonding.
[b] These coordination numbers are obtained by solving equations (11) and (12) together.
[c] These coordination numbers are obtained by solving equation (13) and (14) together taking $C_{Ge}(S) = 4$.
[d] These coordination numbers are obtained from equation (15) (from neutron diffraction).
[e] This situation assumes the Ge atoms would bond to only Ge atoms. These coordination numbers are obtained by solving equations (16) and (17) together taking corresponding $C_{Ge}(S)$ value as a constraint.
[f] This situation assumes the Ge atoms would bond to only As atoms. These coordination numbers are obtained by solving equations (18) and (19) together taking corresponding $C_{Ge}(S)$ value as a constraint.

these glasses equation (7) can be written for neutron as:

$$C^{N} = W^{N}_{AsS} C_{As}(S) + W^{N}_{GeS} C_{Ge}(S) + W^{N}_{AsAs} C_{As}(As). \quad (13)$$

Similarly, for x-ray equation (10) simplifies into the following form in the same range of glass composition:

$$C^{X} = W^{X}_{AsS} C_{As}(S) + W^{X}_{GeS} C_{Ge}(S) + W^{X}_{AsAs} C_{As}(As). \quad (14)$$

The first shell was integrated to obtain the total area under the peaks located at ∼2.2 and ∼2.5 Å for neutron and x-ray diffraction, C^{N} and C^{X}. For this composition range ($20 \leqslant x \leqslant 25$) the coordination numbers for Ge and As atoms can not be readily derived by combining equation (13), and (14) since there are two equations but three unknowns, i.e. $C_{As}(S)$, $C_{Ge}(S)$, and $C_{As}(As)$. Therefore, one needs additional constraints to obtain these coordination numbers. One of the most important yet simple constraints is that in chalcogenide glasses Ge and As atoms are 4 and 3 coordinated, respectively, irrespective of chemical composition [15–17]. Using the constraint $C_{Ge}(S) = 4$ in equations (13), and (14) the number of unknowns can be reduced to two. $C_{As}(S)$ and $C_{As}(As)$ values thus obtained for these glasses by combining neutron and x-ray diffraction are listed in table 4. These values are in good agreement with the corresponding values calculated from glass compositions on the basis of the assumptions that Ge and As atoms are 4 and 3 coordinated, respectively, and that only As atoms take part in metal–metal bonding while Ge atoms are primarily bonded to S atoms.

Previous Ge and As K-edge EXAFS studies have shown that at the highest levels of S-deficiencies ($27.5 \leqslant x \leqslant 33.3$), only Ge atoms take part in heteropolar bonding with S atoms. Therefore, the peak in neutron and x-ray $N(r)$ located at ∼2.2 Å in these glasses corresponds only to Ge–S correlations. For this peak equation (7) can be written as:

$$C^{N} = W^{N}_{GeS} C_{Ge}(S) \quad (15)$$

C^{N} can be obtained by fitting the peak centered at 2.2 Å by a Gaussian function (figure 3(b)). The $C_{Ge}(S)$ values thus obtained are in good agreement with the corresponding average Ge–S coordination numbers obtained in previous Ge K-edge EXAFS studies [15, 16].

For the glasses at the highest levels of S-deficiencies ($27.5 \leqslant x \leqslant 33.3$) the relative degree of chemical order in metal–metal bonding involving Ge and As atoms is not known. Two limiting cases have been considered to understand whether the Ge and As atoms bond randomly or there is any preference for Ge–As bonds over As–As and Ge–Ge bonds. The first structural scenario assumes that the Ge atoms exclusively form Ge–Ge bonds and the second one assumes that metal–metal bonding involving Ge atoms are only of the type Ge–As. For the first case equation (7) can be written for the first shell as:

$$C^{N} = W^{N}_{GeS} C_{Ge}(S) + W^{N}_{AsAs} C_{As}(As) + W^{N}_{GeGe} C_{Ge}(Ge). \quad (16)$$

Similarly, for x-ray diffraction equation (10) takes the form:

$$C^{X} = W^{X}_{GeS} C_{Ge}(S) + W^{X}_{AsAs} C_{As}(As) + W^{X}_{GeGe} C_{Ge}(Ge). \quad (17)$$

Since $C_{Ge}(S)$ values are already known from the solution of equation (15), one can readily solve equations (16), and (17) simultaneously to obtain values of the other two unknowns $C_{As}(As)$ and $C_{Ge}(Ge)$. Applying this methodology results in the Ge and As nearest-neighbor coordination environments listed in table 4 for the glasses with $27.5 \leqslant x \leqslant 33.3$.

For the second case where Ge atoms are assumed to bond only to As atoms, equation (7) can be rewritten as:

$$C^{N} = W^{N}_{GeS} C_{Ge}(S) + W^{N}_{AsAs} C_{As}(As) + W^{N}_{GeAs} C_{Ge}(As). \quad (18)$$

Equation (10) becomes:

$$C^{X} = W^{X}_{GeS} C_{Ge}(S) + W^{X}_{AsAs} C_{As}(As) + W^{X}_{GeAs} C_{Ge}(As). \quad (19)$$

Again, using $C_{Ge}(S)$ values that are already known from the solution of equation (15), one can readily solve equations (18) and (19) simultaneously to obtain values of the other two unknowns $C_{As}(As)$ and $C_{Ge}(As)$. These values are listed in table 4. It is clear from table 4 that both structural scenarios yield sensible coordination numbers for Ge and As atoms (∼4 and 3, respectively). Hence, it is impossible to discern the degree of chemical order associated with metal–metal bonding in these glasses even with combined neutron and x-ray diffraction techniques.

3.2.2. Second shell and the next-nearest-neighbor coordination environments. The peak centered at ∼3.4 Å in the neutron and x-ray total radial distribution functions of the stoichiometric and S-excess glasses, corresponds to Ge/As-Ge/As next-nearest-neighbors that are connected through S atoms i.e. the Ge–S-Ge, As–S–As and Ge–S-As linkages (figures 3, 4). This metal–metal correlation has also been observed in previous Ge and As K-edge EXAFS spectroscopic studies of these glasses [15]. This peak extends asymmetrically out to longer distances and must include significant contribution from nearest-neighbor S–S correlations at ∼3.6 Å in S–Ge–S and S–As–S linkages. This contribution is expected to decrease with increasing S-deficiency as the S–S weighting factors decrease (tables 2a, 2b). The S–S weighting is generally higher for x-rays but has a similar variation with composition for both neutrons and x-rays although at the lowest S contents the x-ray S–S contribution decreases slightly more rapidly than for the neutron case (tables 2a, 2b). These differences in S–S weighting between neutron and x-ray may account for slightly different forms of the respective $N(r)$ functions (figures 3, 4). Increasing S-deficiency results in a progressive shift of the center of gravity of this peak from ∼3.4 to ∼3.8 Å in neutron and x-ray $N(r)$ (figures 3, 4). This shift in the center of gravity is primarily associated with the appearance of metal–metal next-nearest-neighbors linked through another metal atom. These linkages in glasses with low and intermediate levels of S-deficiency ($20 \leqslant x \leqslant 25$) are expected to be primarily of the type As–As–As, since Ge atoms do not participate in metal–metal bonding in these glasses (table 4).

3.2.3. Correlations at $r > 4.0$ Å. For S-excess and stoichiometric glass, a small peak is observed in neutron and x-ray $N(r)$ at ∼4.2 Å that disappears with increasing S-deficiency (figures 3, 4). Both neutron and x-ray $N(r)$ are characterized by a broad peak covering the region between ∼5.0 and 5.5 Å in S-excess and stoichiometric glasses. Increasing S-deficiency results in a progressive shift of the center of gravity of this peak from ∼5.3 to ∼5.7 Å (figures 3, 4). Moreover, peaks at ∼7 Å and ∼9 Å systematically increase in intensity with decreasing S content and become distinct especially in the x-ray $N(r)$ of glasses with the lowest S contents, possibly indicating long-range metal–metal correlations in metal-rich regions (figure 4). Such long-range correlations may primarily arise from As–As pairs since this is the only metal–metal pair for which the x-ray weighting factor is systematically higher than the neutron weighting factor (tables 2a, 2b).

4. Discussion

4.1. Nearest and next-nearest-neighbor coordination environments and short-range order

Combined neutron and x-ray diffraction results show that the nearest-neighbor coordination environments of Ge and As atoms in $Ge_xAs_xS_{100-2x}$ glasses are consistent with the results of previous Ge and As K-edge EXAFS spectroscopic studies [15, 16]. The nearest-neighbor coordination numbers of Ge and As are 4 and 3, respectively, in all glasses irrespective of composition (table 4). In stoichiometric and S-excess glasses the inter-atomic bonding is primarily heteropolar i.e. of the type Ge–S and As–S. The C_{As}(As) values in glasses with $20 \leqslant x \leqslant 25$ derived from the diffraction data are similar to the values expected in these glasses on the basis of their composition and the assumption that Ge atoms do not take part in metal–metal bonding (table 4). Therefore, low and intermediate levels of S-deficiency are accommodated via the formation of homopolar As–As bonds for glasses with $20 \leqslant x \leqslant 25$. Ge atoms start to participate in metal–metal bonding only in the highly S-deficient glasses with $x > 25$, once all the As atoms are used up in homopolar bonding (table 4).

The compositional evolution of the nearest-neighbor coordination environments of Ge and As atoms in these glasses as discussed above is consistent with the corresponding development of short-range order at the next-nearest-neighbor length scales ranging between ∼3 and 4 Å. As mentioned before, the peak in the neutron and x-ray $N(r)$ at ∼3.4 Å in stoichiometric and S-excess glasses is associated with the non-bonded metal–metal distances in heteropolar Ge/As–S-Ge/As linkages (figures 3 and 4). With increasing S-deficiency, this peak position shifts to longer distances ∼3.8 Å corresponding to non-bonded metal–metal distances in homopolar Ge/As–Ge/As–Ge/As linkages. Such next-nearest-neighbor metal–metal distances are in good agreement with the As–As distance of ∼3.76 Å in the As–As–As linkages in crystalline As metal as well as with the As–As distance of 4.0 Å in As–Ge–As linkages in crystalline $GeAs_2$ [28].

4.2. Intermediate-range order

Previous isotope-substituted neutron diffraction and anomalous x-ray scattering studies have shown that the FSDP in chalcogenide glasses arises primarily from metal–metal correlations [29–32]. The nearly linear shift in the position of neutron and x-ray FSDP to lower Q values with increasing S-deficiency imply an increase in the length scale of intermediate-range order in the form of metal–metal correlations (figure 5). For example, the neutron Q_{FSDP} in these glasses decrease from 1.14 to 0.96 $Å^{-1}$ with increasing S-deficiency that indicates a corresponding increase in the length scale of the intermediate-range order from $2\pi/Q_{FSDP} \sim$ 5.5 Å for the S-excess glass to ∼6.5 Å for the most S-deficient glass (table 3, figure 5). This shift in the intermediate-range correlations to longer distances takes place concomitantly with similar shifts in the short-range nearest-neighbor and next-nearest-neighbor correlations from ∼2.2 and 3.4 Å, respectively, to ∼2.5 and 3.8 Å, respectively, with increasing S-deficiency (figures 3, 4, table 4). Therefore, the periodicity in the intermediate-range order as manifested in the position of the FSDP results directly from a propagation of the short-range chemical order in these glasses. Moreover in the highly S-deficient glasses, peaks at ∼7 and ∼9 Å become distinct especially in the x-ray $N(r)$, possibly indicating long-range As–As correlations in metal-rich regions (figure 4).

Increasing S-deficiency results in an increase in the x-ray and neutron FSDP intensities in the composition range $15 \leqslant x \leqslant 25$ and in a decrease in the composition range $25 \leqslant x \leqslant 33.3$ (figure 5). Glasses in these two composition ranges are also characterized by the absence and presence of Ge atoms in metal–metal bonding, respectively (table 4). The FSDP intensity in S-excess and stoichiometric glasses must be related to the intermediate-range metal–metal correlations in the coexisting GeS_2 and As_2S_3 networks. The increase in the FSDP intensity with decreasing S content in the compositional range of $15 \leqslant x \leqslant 18.2$ primarily indicates establishment of intermediate-range metal–metal correlations as the GeS_2 and As_2S_3 networks are fully established in the structure of the stoichiometric glass with $x = 18.2$ (figure 5). A sharp rise in the FSDP intensity with increasing S-deficiency can then be related to additional intermediate-range As–As correlations as As atoms start to participate in homopolar As–As bonding [29]. The coexistence of heteropolar-bonded Ge–S and As–S network and homopolar-bonded As-rich metal clusters in the composition range $18.2 \leqslant x \leqslant 25$ is expected to give rise to strong composition and density fluctuations. This structural scenario is consistent with the increasing intensity of small-angle neutron scattering observed in this compositional range (figure 1(b)). Subsequent rapid drop in FSDP intensity in the compositional range of $25 \leqslant x \leqslant 33.3$ is indicative of the breakdown of intermediate-range correlations in the Ge–S network as Ge starts participating in metal–metal bonding (figure 5) [29]. The glass structure is expected to be dominated by large metal-rich regions at the highest levels of S-deficiency, consistent with the appearance of long-range metal–metal correlation peaks at ∼7 and ∼9 Å in the x-ray $N(r)$ (figure 4). As mentioned earlier, the FSDP in these glasses primarily

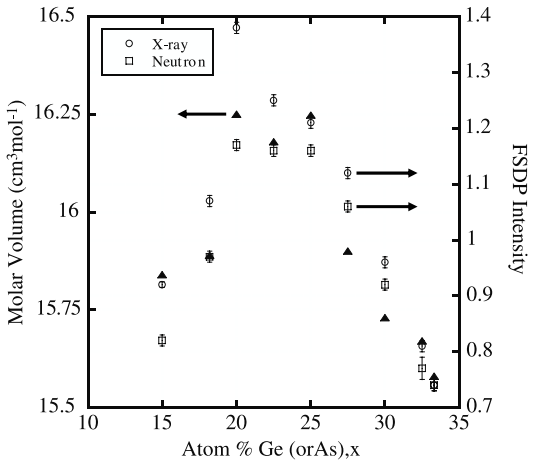

Figure 7. Variation in the amplitude of the neutron and x-ray FSDP (open squares and open circles, respectively) and molar volume (filled triangles) in $Ge_xAs_xS_{100-2x}$ glasses as a function of Ge (or As) content. Molar volume data are from [19] and the corresponding error bars are within the size of the symbols.

arises from metal–metal correlations and the neutron and x-ray Faber–Ziman weighting factors for Ge–Ge, As–As and As–Ge correlations just show a gradual, monotonic increase with increasing metal content (table 2a). Hence, the non-monotonic compositional variation of the FSDP intensity in these glasses cannot be attributed to the compositional changes in the weighting of the partial structure factors.

The compositional variation of the coherence length of intermediate-range order $2\pi/\Delta Q_{\mathrm{FSDP}}$ shows different behaviors in three compositional ranges (figure 6). In the case of the S-excess and stoichiometric glass i.e. for $15 \leqslant x \leqslant 18.2$ the coherence length remains nearly constant at ∼18 Å followed by a rapid increase with increasing S-deficiency to ∼24 Å at $x = 25$ where all As atoms take part in homopolar As–As bonding (figure 6). The coherence length then decreases with further increase in S-deficiency in the compositional region $27.5 \leqslant x \leqslant 33.3$. The rapid increase in coherence length in the compositional region $20 \leqslant x \leqslant 25$ must be related to the formation of homopolar-bonded As-rich clusters in the glass structure. The corner-sharing $AsAs_3$ trigonal pyramids in these clusters may form topologically low-dimensional structural units embedded in a predominantly Ge–S tetrahedral network. Further increase in S-deficiency forces the Ge atoms to participate in metal–metal bonding that interrupts the topological continuity of the As-rich clusters and the Ge–S tetrahedral network which may result in the drop in the coherence length in the compositional region $27.5 \leqslant x \leqslant 33.3$ (figure 6). Finally, previous studies have correlated the intensity of the FSDP with the atomic packing efficiency in glasses [33]. Hence, the intermediate-range structural and topological aspects discussed above are expected to be manifested in the compositional variation of both the FSDP intensity and molar volume of these glasses. It is evident from figure 7 that FSDP intensity and molar volume of these glasses are in fact strongly correlated and indeed both go through a maximum in glasses with $x \sim 25$ that are characterized by the presence of the homopolar-bonded As clusters.

5. Conclusion

The coordination environments of Ge and As atoms in $Ge_xAs_xS_{100-2x}$ glasses are determined using combined neutron diffraction and x-ray diffraction experiments and are found to be consistent with our earlier results based on Ge and As K-edge EXAFS spectroscopic studies. Ge and As atoms are primarily heteropolar bonded to S atoms in stoichiometric and S-excess glasses. Formation of homopolar As–As bonds at low and intermediate levels of S-deficiency results in violation of chemical order and in the formation of As-rich structural moieties. Ge takes part in metal–metal bonding only in the highly S-deficient glasses once all the As atoms are used up in homopolar bonding. This short-range order, at length scales ranging between 2 and 4 Å, propagates into progressive shift in the longer-range metal–metal correlations from 5.3 to 5.7 Å with increasing S-deficiency that results in systematic changes in atomic packing and shift in FSDP position as a function of composition. Metal–metal correlations at ∼7 and 9 Å in metal-rich regions become prominent in glasses with highest levels of S-deficiency. This intermediate-range ordering and its topological influence on atomic packing are manifested in the compositional variation of the coherence length of intermediate-range order and of the amplitude of the FSDP.

Acknowledgments

This work was supported by the National Science Foundation grant DMR 0603933 to SS. The IPNS Division, Argonne National Laboratory is supported by the US DOE under contract number DE-AC02-06CH11357.

References

[1] Sanghera J S and Aggarwal I D 1999 *J. Non-Cryst. Solids* **256/257** 6
[2] Seddon A B 1995 *J. Non-Cryst. Solids* **184** 44
[3] Shimakawa K, Kolobov A V and Elliott S R 1995 *Adv. Phys.* **44** 475
[4] Greaves G N and Sen S 2007 *Adv. Phys.* **56** 1
[5] Eckert H 1994 *NMR Basic Principles and Progress* vol 33 ed P Diehl, E Fluck, H Günther, R Kosfeld and J Seelig (Berlin: Springer) p 125
[6] Lowe A J, Elliott S R and Greaves G N 1986 *Phil. Mag.* B **54** 483
[7] Zhou W, Paesler M A and Sayers D E 1992 *Phys. Rev.* B **46** 3817
[8] King W A, Clare A G, LaCourse W C, Volin K, Wright A C and Wanless A 1997 *J. Phys. Chem. Glasses* **38** 269
[9] Armand P, Ibanez A, Dexpert H and Philippot E 1992 *J. Non-Cryst. Solids* **139** 137
[10] Jackson K, Briley A, Grossman S, Porezag D V and Pederson M R 1999 *Phys. Rev.* B **60** R14985
[11] Zhou W, Paesler M A and Sayers D E 1991 *Phys. Rev.* B **43** 2315
[12] Petri I, Salmon P S and Fischer H E 2000 *Phys. Rev. Lett.* **84** 2413

[13] Bureau B, Troles J, Le Floch M, Guenot P, Smektala F and Lucas J 2003 *J. Non-Cryst. Solids* **319** 145
[14] Bureau B, Troles J, Le Floch M, Smektala F and Lucas J 2003 *J. Non-Cryst. Solids* **326/327** 58
[15] Sen S, Ponader C W and Aitken B G 2001 *J. Non-Cryst. Solids* **293–295** 204
[16] Sen S, Ponader C W and Aitken B G 2001 *Phys. Rev.* B **64** 104202
[17] Sen S and Aitken B G 2002 *Phys. Rev.* B **66** 134204
[18] Aitken B G and Ponader C W 1999 *J. Non-Cryst. Solids* **256/257** 143
[19] Aitken B G and Ponader C W 2000 *J. Non-Cryst. Solids* **274** 124
[20] Lippens P E, Jumas J C, Olivier-Fourcade J and Aldon L 2000 *J. Non-Cryst. Solids* **271** 119
[21] Ellison A J G, Crawford R K, Montague D G, Volin K J and Price D L 1993 *J. Neutron Res.* **4** 61
[22] Soper A K, Howells W S and Hannon A C 1989 ATLAS-analysis of time of flight diffraction data from liquid amorphous samples *Technical Report RAL 89-046* Rutherford Appleton Laboratory, Chilton, Oxon, UK
See also: Urquidi J, Benmore C J, Neuefeind J and Tomberli B 2003 *J. Appl. Crystallogr.* **36** 368
[23] Sears V F 1986 *Neutron Scattering* (*Methods of Experimental Physics*) vol 23, ed K Skold and D L Price (Orlando, FL: Academic) p 521 Part A
[24] Lorch E A 1969 *J. Phys. C: Solid State Phys.* **2** 229
[25] Chantler C T 1995 *J. Phys. Chem. Ref. Data* **24** 71
[26] Susman S, Volin K J, Montague D G and Price D L 1990 *J. Non-Cryst. Solids* **125** 168
[27] Leadbetter A J and Wright A C 1972 *J. Non-Cryst. Solids* **7** 23
[28] Bryden J H 1962 *Acta Crystallogr.* **15** 167
[29] Bychkov E, Benmore C J and Price D L 2005 *Phys. Rev.* B **72** 172107
[30] Arai M, Johnson R W, Price D L, Susman S, Gay M and Enderby J E 1986 *J. Non-Cryst. Solids* **83** 80
[31] Petri I, Salmon P S and Fischer H E 2000 *Phys. Rev. Lett.* **84** 2413
[32] Eisenbergen H, Fuoss P, Warburton W K and Bienenstock A 1981 *Phys. Rev. Lett.* **46** 1537
Barnes A C *et al* 1999 *J. Non-Cryst. Solids* **250–252** 393
[33] Elliott S R 1991 *Phys. Rev. Lett.* **67** 711